

# Mechanical properties and acoustic emission characteristics of thick hard roof sandstone in Shendong coal field

Huigui Li<sup>1,2</sup> · Huamin Li<sup>1,2</sup>

Received: 23 August 2016/Revised: 21 December 2016/Accepted: 7 March 2017/Published online: 16 March 2017  
© The Author(s) 2017. This article is an open access publication

**Abstract** The mechanical properties and acoustic emission characteristics of thick hard roof sandstone were investigated. Samples were taken from the 30.87-m thick sandstone roof in a mine in the Shendong coal field, China. Firstly, the composition and microscopic characteristics were analyzed by XRD and FE-SEM, respectively. Moreover, the indirect tensile test, uniaxial compression test, three axis compression experiment and AE test are carried out by using RMT-150C mechanics experiment system with DS5-8B AE test system. The experiment results indicate that the main framework particles of sandstone are quartz and feldspar, and mainly quartz. Cements are mainly pyrite, kaolinite, chlorite and zeolite cross needle, clinocllore, and clay minerals. The microstructure of sandstone is very dense, with few pores and high cementation degree. The tensile strength, compressive strength and elastic modulus of sandstone are 4.825, 85.313 MPa, 13.814 GPa, respectively, so the sandstone belongs to hard rock. The AE cumulative counts of sandstone can be divided into three phases: relatively flat growth period, rapid growth period and spurt period. The signal strength of AE waveform can be used as a warning signal. In the tensile fracture zone, the warning value is 0.4 mV, and in the compression shear failure zone, it is 4 mV. The numbers of cumulative counts of AE under different stress conditions have obvious difference. Moreover, the growth of cumulative counts of acoustic emission is more obvious when the stress is more than 60% of the peak stress.

**Keywords** Mechanical · Acoustic emission (AE) · Sandstone · X-ray diffractometer (XRD) · Field emission scanning electron microscope (FE-SEM)

## 1 Introduction

The Daliuta coal mine is a large modern mine in the Shenhua coal group, with approved production capacity of 21,700,000 tons. The Shenhua coal group is located in the northern part of Shaanxi Province and composed of the

Daliuta and Huojitu coal mines. Daliuta has mine area of 189.9 km<sup>2</sup>, coal reserves of 2.32 billion tons, and recoverable reserves of 1.53 billion tons. The roof of the 5–2 coal seam is composed of sandstone with an average thickness of 30.87 m. In order to prevent the roof failure due to weighting over great extent, pre splitting blasting for the thick sandstone in the open cut hole was carried out. However, the initial pressure occurs until the panel advances to the 95 m. Such a large area of the roof once falling will cause great harm. This is a serious threat to the safety and efficiency of production on the working face. Therefore, it is urgent to find out the internal cause of roof failure due to weighting over great extent, so that the corresponding control measures can be put forward. According to the formation of this kind of mine pressure, the rock mechanical properties of the overlying strata are

---

✉ Huigui Li  
lihuigui1221@163.com

<sup>1</sup> School of Energy Science and Engineering, Henan Polytechnic University, Jiaozuo 454000, Henan, People's Republic of China

<sup>2</sup> Opening Project of Key Laboratory of Deep Mine Construction, Henan Polytechnic University, Jiaozuo 454000, Henan, People's Republic of China

the major influential factors. Moreover, acoustic emission monitoring can monitor and predict this kind of dynamic disaster. Therefore, it has engineering and theoretical significance to study the mechanics and acoustic emission characteristics of the rock.

Domestic and foreign scholars have well studied the mechanical properties and AE characteristics of rock and made outstanding contributions to the advancement of rock mechanics and acoustics. The structural plane has an important influence on the mechanical and acoustic emission characteristics of rock. Scholars carried out laboratory experiments and numerical simulations on rocks with structural plane. Meanwhile, the relationship among the structural plane, mechanical properties, and acoustic emission characteristics was also established (Liu et al. 2012; Wang et al. 2013; Han and Zhang 2014; Su et al. 2014; Yang et al. 2014; Zhu et al. 2015). Some scholars have studied the mechanics and damage characteristics of sandy mudstone, metamorphic quartz sandstone and silty sandstone under triaxial compression and triaxial unloading confining pressure (Fang et al. 2015; Deng et al. 2016; Guo et al. 2016). The mechanical properties and acoustic emission characteristics of sandstone under impact loading were studied by (Li 2014; Zhang et al. 2014; Li et al. 2015a, b; Liu et al. 2015). Besides, they explored the effect of strain rate on the mechanical properties and acoustic emission characteristics of sandstone under impact loading. Water also has an important effect on the physical properties, mechanical properties, and acoustic emission characteristics of rock. The effects of water on the physical and mechanical properties and acoustic emission characteristics of silty sandstone, coal and sandstone were analyzed by other researchers (Chen et al. 2013; Deng et al. 2014; Gao et al. 2015a, b; Zhang et al. 2015, 2016), and the results indicate that water can significantly alter the wave velocity, compressive strength, elastic modulus, failure pattern and acoustic emission characteristics of coal and rock. The effect of pore pressure and confining pressure on short-term and creep mechanical behavior of saturated and dry red sandstone were studied by Yang et al. (2015). The effect of strain rate on the mechanical behavior of sandstone with different grain sizes was studied by Wasantha et al. (2015). The microscopic damage and dynamic mechanical characteristics of rock under the freeze–thaw environment were studied by Zhou et al. (2015).

However, studies on the mechanical properties and acoustic emission characteristics of thick hard roof sandstone are scarce. In order to explore the internal cause of dynamic disasters such as the formation of shock, and take corresponding control measures, the mechanical properties and acoustic emission characteristics of the thick hard roof sandstone in the Shendong coal field were studied

experimentally and the results are analyzed and discussed in this paper.

## 2 Experimental

### 2.1 Sample preparation

The panel of 52307 extracts 5–2 coal seam. The roof of the 5–2 coal seam is composed of sandstone with an average thickness of 30.87 m, as shown in Table 1. In order to study the mechanical properties and acoustic emission characteristics of the sandstone, the method of core drilling was used in the process of sampling. All the collected samples were wrapped by foam, and then put into a core box for protection during the transportation. According to the requirements of regulation (the Ministry of Water Resources of P. R. China 2008), the Brazil split and the uniaxial and triaxial compression tests samples should be processed into  $\phi 25 \text{ mm} \times 25 \text{ mm}$ ,  $\phi 50 \text{ mm} \times 100 \text{ mm}$  respectively.

### 2.2 Testing equipment

Uniaxial compression test, indirect tensile test and triaxial compression test were carried out on a RMT-150C mechanical testing machine. The system is composed of main control computer, hydraulic controller, three axial pressure sources, digital controller, manual controller, hydraulic actuator and hydraulic source. The acoustic emission test was carried out with a DS5 acoustic emission monitor. The system has 8 channels and can monitor the external parameters such as temperature and pressure. Moreover, the system can identify the location of acoustic emission and record the waveform characteristics in the whole experiment process.

### 2.3 Testing procedure

#### (1) AE test

The AE test is applied with the mechanics experiment simultaneously. The experiment system diagram is shown

**Table 1** Lithological characteristics of the seam roof

Lithology	Thick (m)	Depth (m)
Fine sandstone	30.87	175.62
Siltstone	0.60	176.22
Medium sandstone	0.70	176.92
Siltstone	2.41	179.33
5–2 coal	7.04	186.37

in Fig. 1. In the AE test, two probes are symmetrically placed in the middle of the sample. In order to maintain the full contact of the sensor and the sample, the sensor is coated with a coupling agent in the test process. During the experiment, the AE system and the mechanics experiment system begin to collect the data simultaneously. The external parameter of the AE test is 40 dB, the threshold value is 50 mv, and the sampling frequency is 3 MHz.

(2) Mechanics experiment

The indirect tensile test adopts force control at the loading rate of 0.2 kN/s, which is repeated for 5 samples. And the uniaxial compression test adopts displacement control at the loading rate of 0.005 mm/s, which is repeated for 3 samples.

Triaxial compression experiment is controlled by displacement. Firstly, loading confining pressure to 5,10,15,20 and 25 MPa by the loading rate of 0.5 MPa/s, under the condition of hydrostatic pressure which turns to be  $\sigma_1 = \sigma_2 = \sigma_3$ . Then continue loading axial compression by the loading rate of 0.01 mm/s while keeping confining pressure constant till the specimens get destroyed. During the test, the axial loading and acoustic emission testing are kept simultaneously.

### 3 Composition and microstructure characteristics

#### 3.1 Analysis of mineral composition

Many methods have been used to examine the microfabric of rock (Sachan and Penumadu 2007; Yao et al. 2016). In this study, the method of X-ray diffractometer is used to study the mineral composition of the roof sandstone, and the results are shown in Table 1 and Fig. 2. Table 2

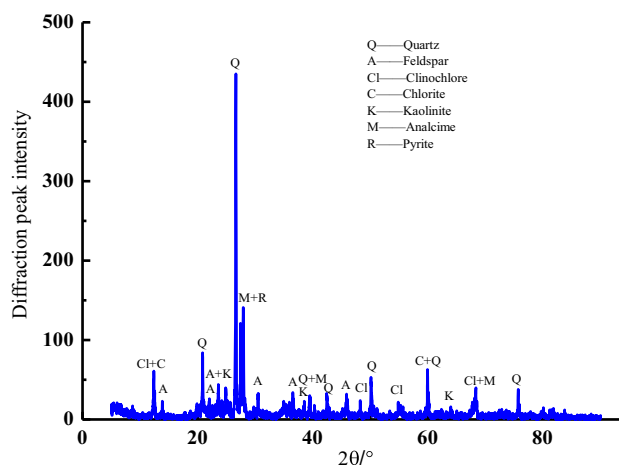


Fig. 2 X-ray diffraction analysis of roof sandstone

indicates that the framework grain of thick hard roof sandstone is quartz and feldspar, constituting about 69.7% of the total mass. Cements mainly have pyrite, kaolinite, chlorite, zeolite cross needle and clinocllore, and the main cement components are clay minerals constituting about 20.8% of the total mass.

#### 3.2 Microstructure characteristics

The microstructure of samples was analyzed by a field emission scanning electron microscope. The images of the roof sandstone are enlarged 100, 200, 500, 1000, 2000 and 5000 times. The SEM images of 500 times and 2000 times are shown in Fig. 3. The figure indicates that the sandstone has a very dense structure, fuzzy boundaries, few pores, highest degree of cementation, abundant clay minerals and mineral Si surrounded very closely by clay minerals.

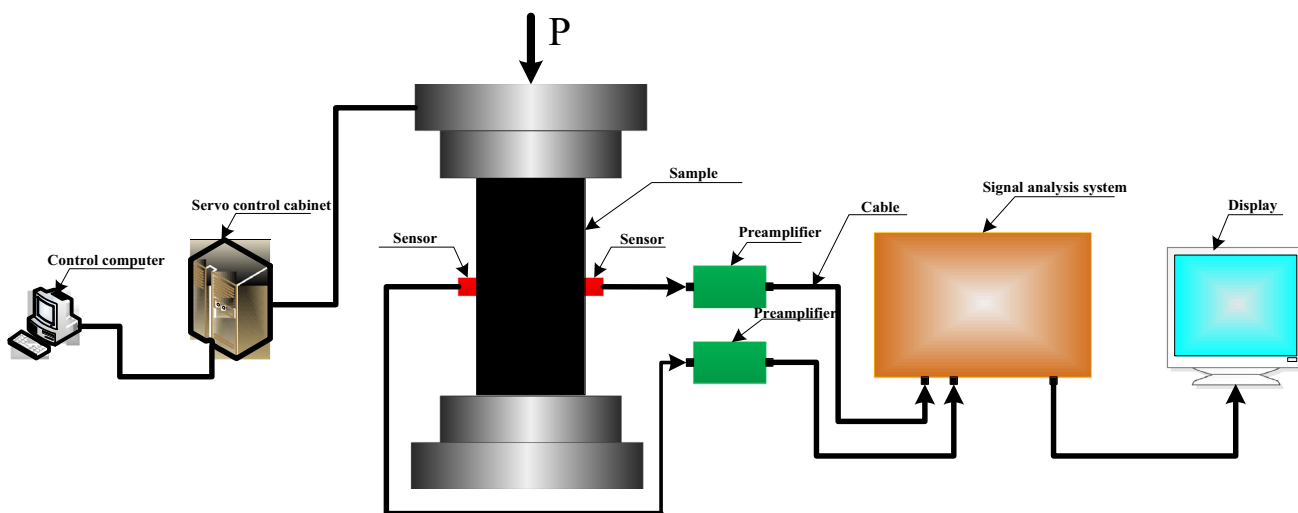
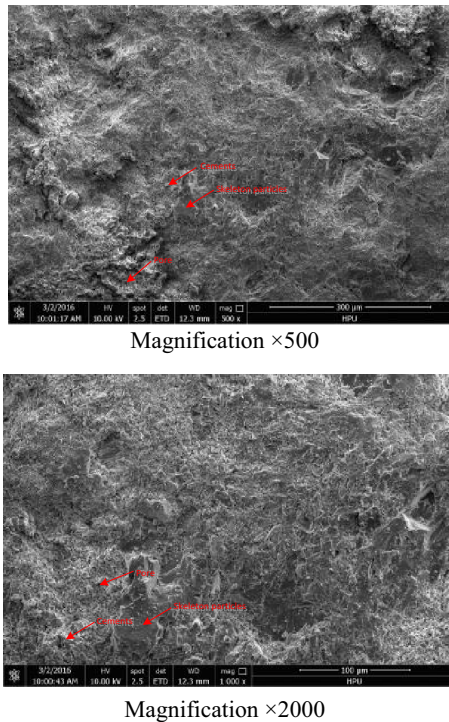


Fig. 1 Figure of test system

**Table 2** Analysis result of component

Sample	Mineral components (%)						
	Quartz	Feldspar	Kaolinite	Pyrite	Chlorite	Clinochlore	Analcime
Sandstone	42.6	27.1	13.5	1.7	0.1	7.2	7.9

**Fig. 3** Scanning electron microscope results of roof sandstone

## 4 Mechanical properties

In order to study the mechanical properties of thick roof sandstone, the indirect tensile test, uniaxial compression test and triaxial compression test were carried out, respectively (Fig. 4).

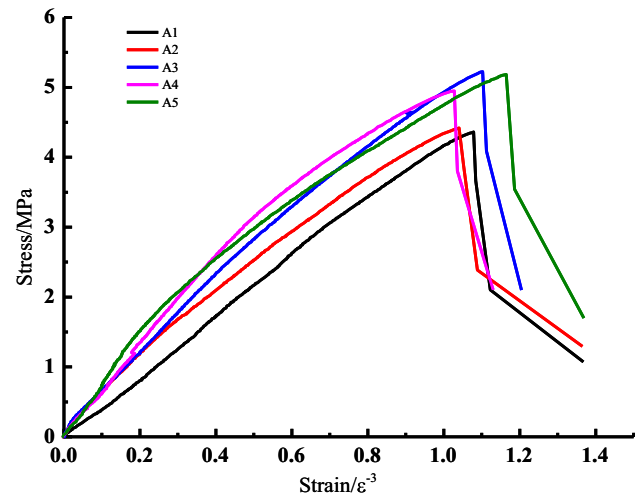
### 4.1 Analysis of the results of indirect tensile test

The damage of roof is not only caused by compression and shear failure, but also by tensile failure. The yield tensile strength and peak tensile strength of the sample are calculated by (1).

$$R = \frac{2P}{\pi DL} \quad (1)$$

where,  $P$  is load, N;  $D$  is diameter of the sample, mm;  $L$  is the height of the sample, mm.

Table 3 lists the mechanical parameters of sandstone under indirect tension. Figure 4 shows the stress–strain curves of sandstone under indirect tension. The tensile strength of roof sandstone ranges from 4.360–5.228 MPa,

**Fig. 4** Stress–strain curves of sandstone under indirect tension

with the average of 4.825 MPa. The peak strain of roof sandstone is in the range of  $1.028 \times 10^{-3}$ – $1.165 \times 10^{-3}$ .

### 4.2 Analysis of the results of uniaxial compression test

Uniaxial compression tests were carried out to obtain the mechanical parameters (such as the compressive strength, elastic modulus and Poisson's ratio) of the samples of roof sandstone. The test results and derived mechanical parameters are shown in Table 4. Figure 5 shows the stress–strain curves of sandstone under uniaxial compression. Table 4 indicates that the uniaxial compressive strength and elastic modulus of roof sandstone are relatively high. The range of peak stress is 81.779–89.175 MPa with an average value of 85.313 MPa. According to the definition in regulation (the Ministry of Water Resources of P. R. China 2008), sandstone is a hard rock. The range of peak strain is  $7.229 \times 10^{-3}$ – $8.331 \times 10^{-3}$ , with an average value of  $7.929 \times 10^{-3}$ . The range of elasticity modulus is 12.951–15.155 GPa, with an average value of 13.814 GPa.

### 4.3 Analysis of the results of triaxial compression test

Five standard samples were chosen to carry out the conventional triaxial compression test to obtain the parameters of cohesion and internal friction angle. According to the

**Table 3** Mechanical parameters of sandstone in indirect tension

Serial number	Diameter (mm)	Height (mm)	Loading rate (kN/s)	Tensile strength (MPa)	Strain ( $10^{-3}$ )
A1	49.80	25.30	0.2	4.360	1.078
A2	49.82	25.92	0.2	4.413	1.041
A3	49.82	26.36	0.2	5.228	1.103
A4	49.92	26.02	0.2	4.939	1.028
A5	49.90	27.90	0.2	5.183	1.165

requirements in regulation, five specimens were tested under the confining pressure of 5, 10, 15, 20 and 25 MPa. Displacement control was adopted in the experiment. The rate of axial loading was 0.002 mm/s and the rate of confining pressure loading was 0.5 MPa/s. The condition of hydrostatic pressure ( $\sigma_1 = \sigma_2 = \sigma_3$ ) was adopted at the initial stage of triaxial compressive loading. Table 5 shows the mechanical parameters of sandstone under different confining pressure. The variables  $\sigma_1$ ,  $\sigma_3$ ,  $E$  and  $\varepsilon_0$  represent the peak stress, confining pressure, modulus of elasticity and peak strain, respectively. Figure 6 shows the stress-strain curve of roof sandstone under different confining pressure. Based on the mechanical parameters under different confining pressures, the cohesive force and the internal friction angle were derived to be 23.389 MPa and  $32^\circ$ , respectively.

Figures 5 and 6 indicate that the test process of uniaxial and triaxial compression can be divided into the

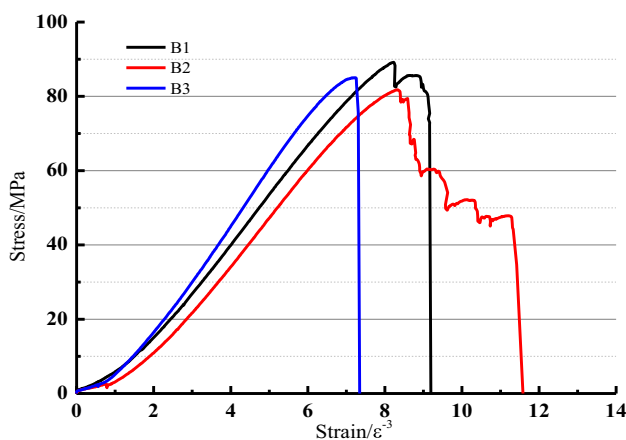


**Fig. 5** The stress-strain curves of sandstone under uniaxial compression

**Table 4** Mechanical parameters of sandstone under uniaxial compression

Serial number	Diameter (mm)	Length (mm)	Loading rate(kN/s)	Stress (MPa)	Strain ( $10^{-3}$ )	Elasticity modulus (GPa)	Poisson's ratio
B1	49.70	99.82	0.005	89.175	8.227	13.336	0.249
B2	50.20	100.70	0.005	81.779	8.331	12.951	0.273
B3	50.02	100.40	0.005	84.984	7.229	15.155	0.239

compaction phase, linear elastic phase, yield phase and failure phase. In uniaxial compression, the compression phase is relatively long, and the yield phase is short. After the peak stress is reached, the stress drops rapidly, suggesting the brittle characteristics of roof sandstone. However, with the increase of confining pressure, the stage of compaction becomes shorter and the peak strain increases gradually. After the peak stress is reached, the stress drops at a lower rate, and the sandstone is gradually transformed from brittle to ductile.

### 5 Acoustic emission characteristics

AE is a phenomenon caused by partial fracture of rock material and rapid release of energy in the form of elastic wave (Gao et al. 2015a, b; Li et al. 2015a, b). In the fracturing process of thick hard roof sandstone in the Shendong coal field, energy will be quickly released in the form of elastic wave. Therefore, the characteristics of acoustic emission may provide precursor information during the fracturing process of hard roof and help to the monitor and predict potential dynamic disaster of hard roof.

In this study, the AE signals were monitored in the indirect tensile test, uniaxial compression test and triaxial compression test. The AE counts, cumulative counts of AE and waveform characteristics were obtained as the results of the acoustic emission test.

#### 5.1 Analysis of acoustic emission count and cumulative count characteristics

Figures 7, 8, 9 show the relationship curves among the acoustics emission count, cumulative count, and stress in the roof sandstone during the course of the indirect tensile

**Table 5** Mechanical parameter of sandstone under different confining pressure

Serial number	Diameter (mm)	Length (mm)	$\sigma_3$ (MPa)	$\sigma_1$ (MPa)	Strain ( $10^{-3}$ )	$E$ (GPa)
C1	50.02	98.86	5	103.663	10.563	13.813
C2	50.06	100.40	10	114.277	9.388	14.874
C3	50.02	100.38	15	136.319	12.637	12.816
C4	50.02	99.70	20	138.507	13.832	12.166
C5	50.02	100.10	25	173.503	15.446	15.771

test, uniaxial compression test and triaxial compression test. The acoustic emission characteristics during the indirect tensile test, uniaxial compression test and triaxial compression test can be divided into three phases: (1) relative flat growth of the cumulative counts of acoustic emission, (2) rapid growth of the cumulative counts of acoustic emission and (3) spurt of the cumulative counts of acoustic emission. The first phase is particularly evident in the indirect tensile test: acoustic emission appears rarely,

and the peak of acoustic emission counts is particularly small. However, acoustic emission appears frequently, and the peak of acoustic emission counts is particularly large during the triaxial compression test. This phenomenon is caused by confining pressure. In the second phase, the frequency of acoustics emission counts appears to gradually increase, and the peak count of acoustics emission gradually increases. In the third phase, the frequency of acoustic emission counts appears very high. Moreover, the peak of acoustic emission counts is larger than those in the first two phases. Especially on the eve of fracture, the acoustic emission count will appear a peak. The peak value of acoustic emission count of sandstone in the uniaxial compression is especially obvious.

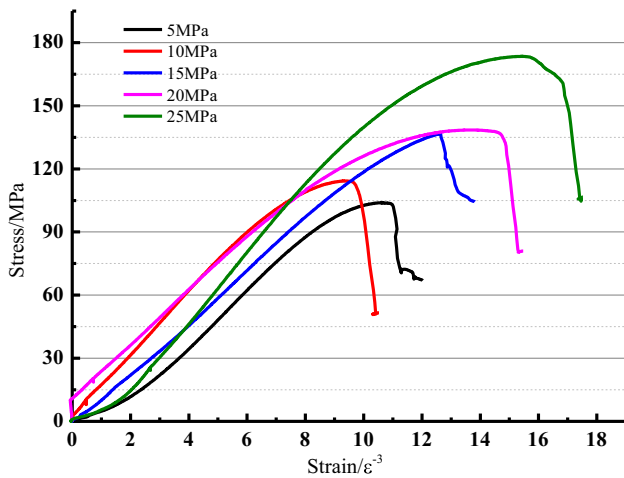


**Fig. 6** Stress-strain curves of sandstone under different confining pressure

**5.2 Analysis of the characteristics of acoustic emission waveform**

In order to study the precursor information of acoustic emission during the fracturing of hard roof, the characteristics of the acoustic emission waveform in the indirect tensile test, uniaxial compression test and triaxial compression test were investigated. It can be seen in Figs. 10, 11 that in the phases with relatively flat growth and rapid growth of cumulative counts, the intensity of the acoustic emission signal is relatively small. However, after entering the spurt phase, the signal intensity gradually increases. In the indirect tensile test, the increase of acoustic emission

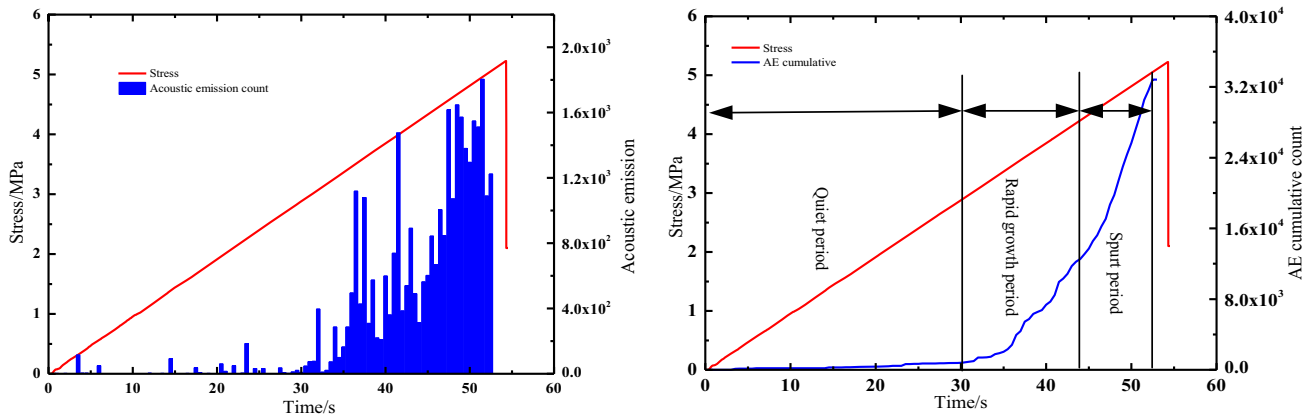


**Fig. 7** Relationship among AE counts, cumulative counts, stress with time of sandstone in indirect tensile test

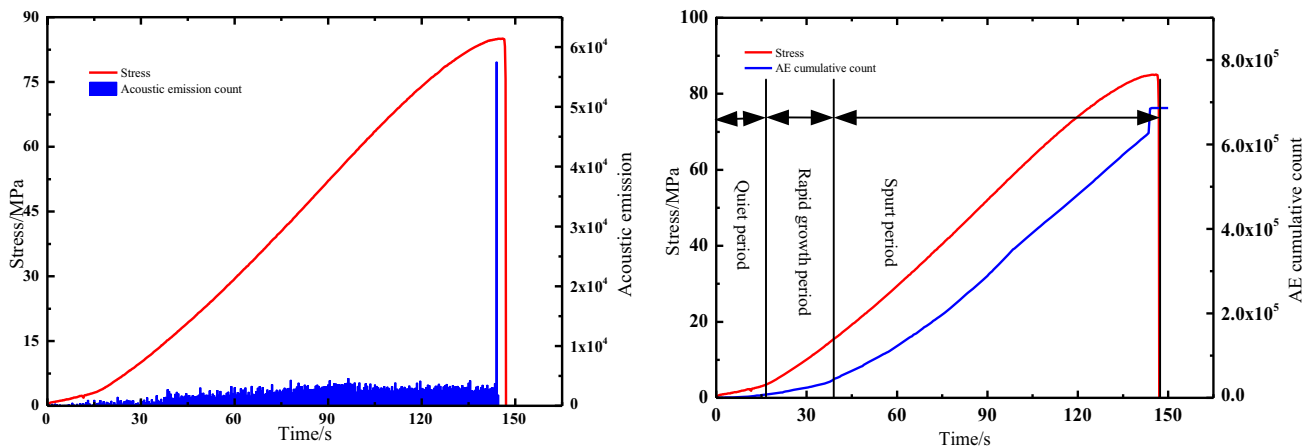


Fig. 8 Relationship among AE counts, cumulative counts, stress with time of sandstone in uniaxial compression test

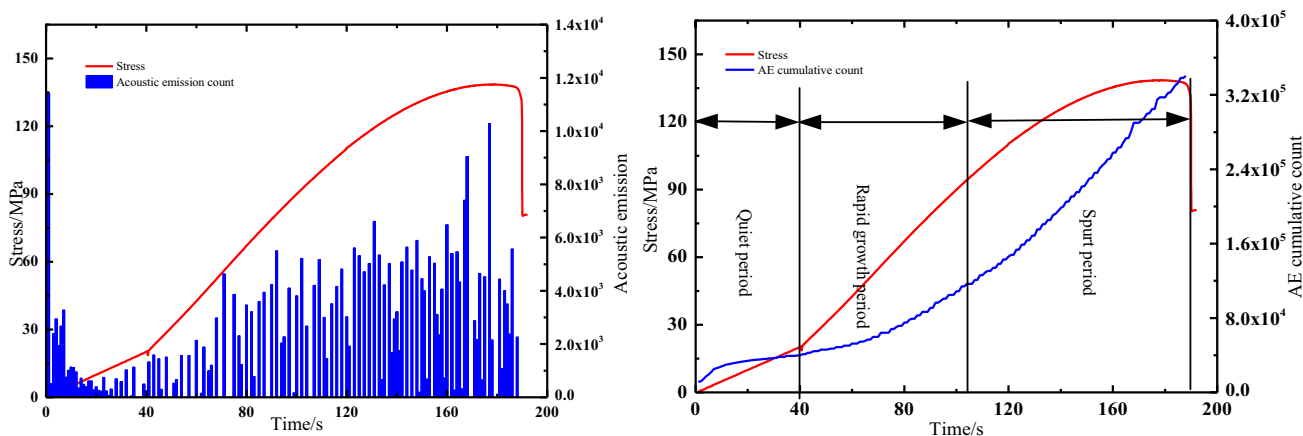


Fig. 9 Relationship among AE counts, cumulative counts, stress with time of sandstone in triaxial compression test

signal intensity is not obvious, but it is particularly obvious during the uniaxial compression test. The peak signal intensity is 10 times of those in the first two phases. In particular, right before the occurrence of fracture, the peak signal intensity is 25 times of those in the first two phases. Therefore, the signal intensity of the warning line can be set to be  $\pm 0.4$  mV in the tensile fracture zone. When the absolute value of the signal intensity is more than 0.4 mV, early warning signal is sent out. The signal intensity of the warning line can be set to  $\pm 4$  mV in the compression shear fracture zone. When the absolute value of the signal intensity is more than 4 mV, early warning signal is sent out.

### 5.3 Analysis of the characteristics of acoustic emission under different stress conditions

The acoustic emission characteristics vary under different stress conditions, and knowledge about the pattern of variation may help to find proper precursor information.

The whole process of acoustic emission count is divided into 10 stages to analyze the acoustic emission characteristics of roof sandstone under different stress stages, the stress of 0%–10%, 10%–20%, 20%–30%, 30%–40%, 40%–50%, 50%–60%, 60%–70%, 70%–80%, 80%–90% and 90%–100%, respectively. Table 6 and Fig. 12 show that the acoustic emission count of roof sandstone has great difference under different stress conditions. In the indirect tensile test, before 60% peak tensile strength is reached, the frequency of acoustic emission count appears very low. The range of acoustic emission counts is 0.15%–1.99%. In the uniaxial compression test, before 60% peak tensile strength is reached, the number of acoustic emission counts is less than 10% of the whole process. The range of acoustic emission counts is 3.04%–9.65%. In the triaxial compression test, the frequency of acoustic emission counts appears very high in the first stage. However, from the second stage to the 80% peak stress, the number of acoustic emission counts is less than 10% of the whole process.

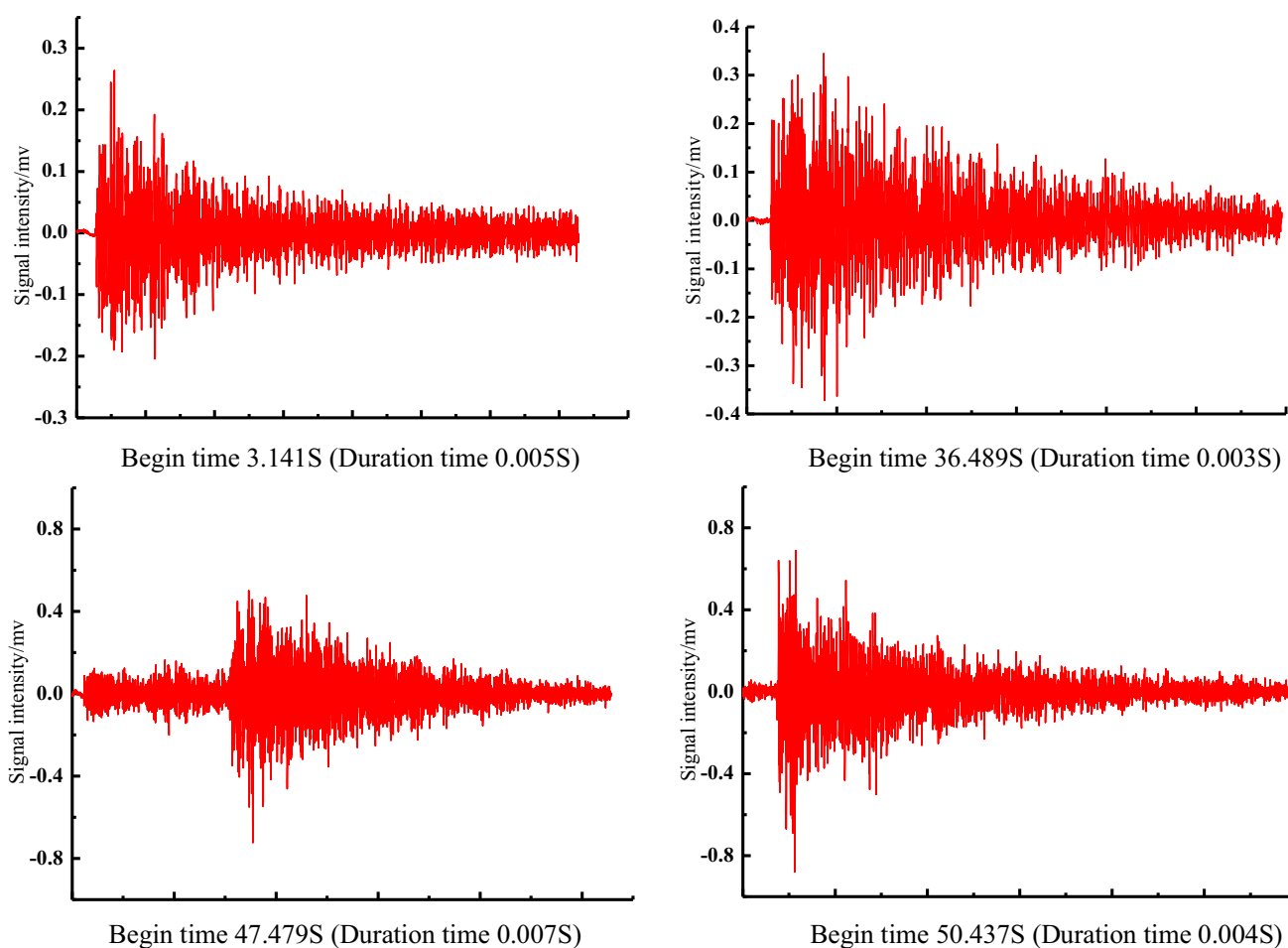


**Fig. 10** Waveform characteristics of acoustic emission in different stages of roof sandstone under the indirect tensile test

## 6 Engineering significance

Effective monitoring, prediction, prevention and control measures of roof dynamic disasters have always been a hot and difficult research topic. At present, displacement and pressure monitoring are commonly used to alert the dynamic disaster of roof. The operation method is simple and easy to master, but the method needs to consume a lot of manpower and material resources. Moreover, continuous and real-time monitoring can not be realized. However, the characteristics of rock mass structures can be reflected in the number of acoustic emission counts, cumulative counts and waveform characteristics in the fracturing process of rock mass. Continuous and real-time monitoring can be carried out by using the AE inspect. Therefore, acoustic emission monitoring provides another way for the prevention of roof dynamic disasters. According to the analyses in Sects. 5.1, 5.2 and 5.3, the AE counts, cumulative counts, AE signal intensity and the acoustic emission cumulative counts under different stress conditions are closely related to the fracturing process of the roof

sandstone. Therefore, a prediction system of roof dynamic disaster is established based on the analyses in Sects. 5.1, 5.2 and 5.3, and the technical route is shown in Fig. 13.

The monitoring and prevention technology of roof power disaster mainly includes the following steps:

- (1) Reasonable selection of the location of the measuring point;
- (2) To determine that the test point is in the tensile fracture zone or compressive shear failure zone;
- (3) Based on the AE counts, determine whether the partition is reasonable;
- (4) This is mainly based on the number of the acoustic emission counts and the frequency of occurrence to determine the partition is reasonable. If the acoustic emission count in the tensile fracture zone is basically greater than 1000, the division is not reasonable.
- (5) Based on the monitoring of acoustic emission parameters, determine whether it is more than the warning value, if more than the warning value, send out an early warning signal.



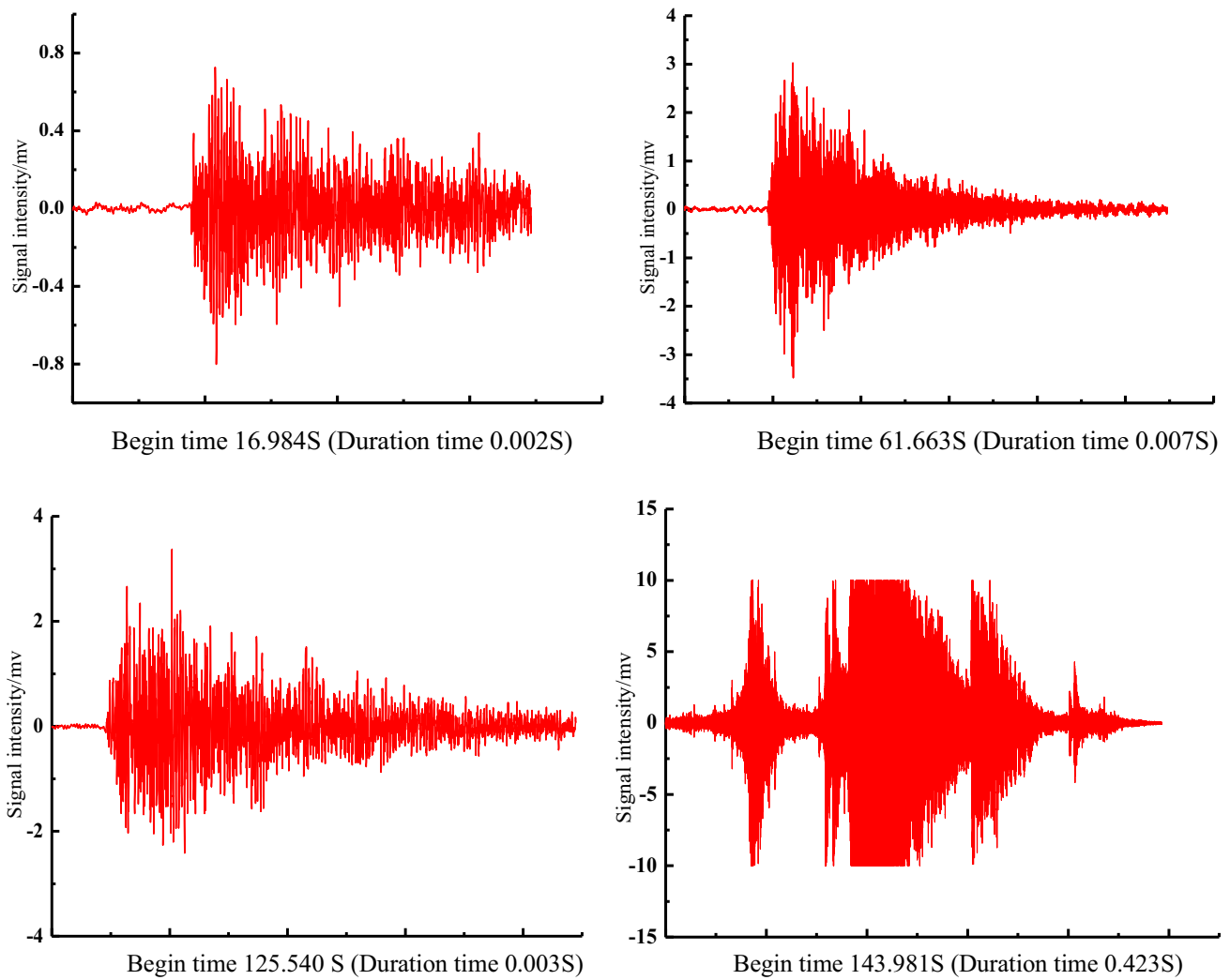


**Fig. 11** Waveform characteristics of acoustic emission in different stages of roof sandstone under the uniaxial compression test

**Table 6** Acoustic emission characteristics of sandstone under different stress stages

Stress phase (%)	Indirect tensile test		Uniaxial compression test		Triaxial compression test	
	AE count	Percent (%)	AE count	Percent (%)	AE count	Percent (%)
0–10	130	0.40	20875	3.04	36360	11.46
10–20	49	0.15	30923	4.50	8122	2.56
20–30	103	0.31	47347	6.90	5841	1.84
30–40	174	0.53	53075	7.73	9351	2.95
40–50	289	0.88	60937	8.88	15495	4.88
50–60	653	1.99	66284	9.65	21262	6.70
60–70	4359	13.27	77996	11.36	23524	7.41
70–80	6482	19.74	68875	10.03	26008	8.19
80–90	10054	30.62	77877	11.34	44543	14.03
90–100	10546	32.11	182360	26.56	126865	39.97

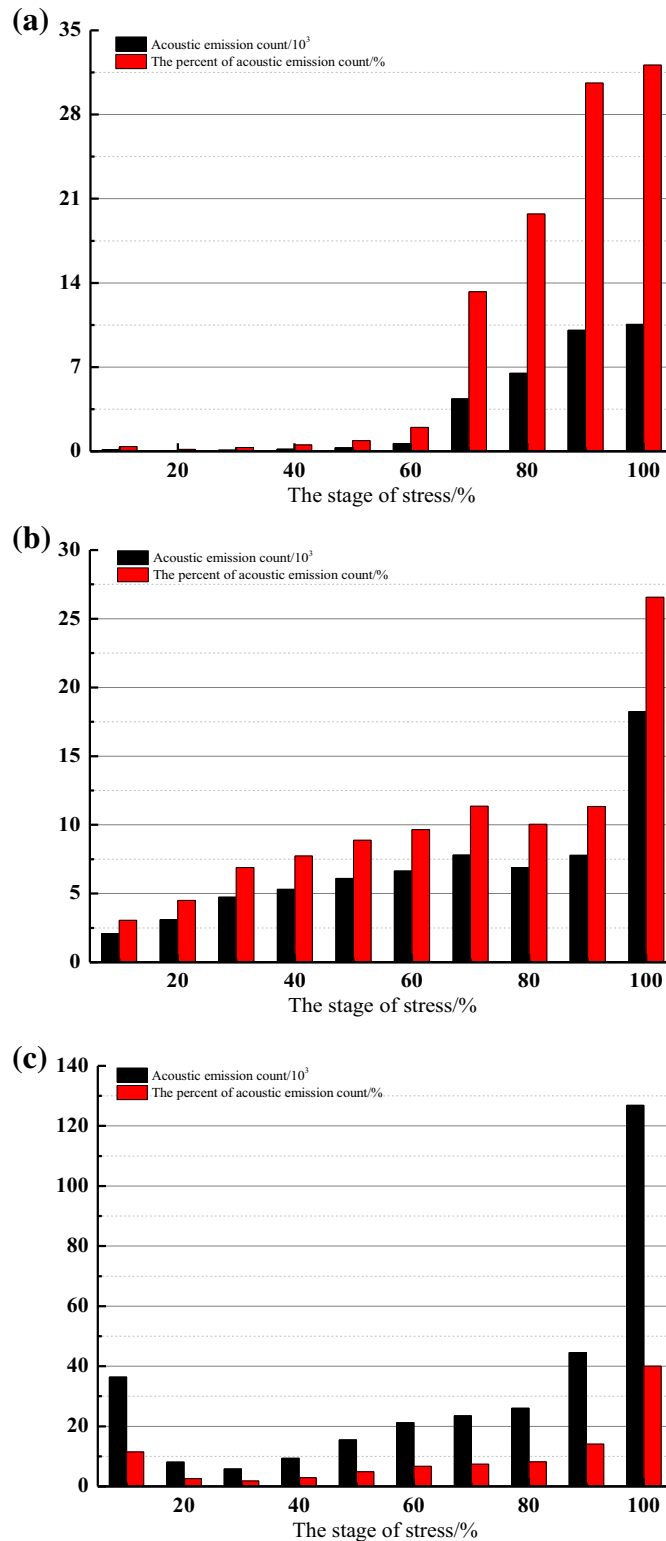


**Fig. 12** Acoustic emission characteristics of sandstone under different stress stages. **a** Indirect tensile test, **b** uniaxial compression test, **c** triaxial compression test

(6) Determine whether the pre-warning information is reliable according to the early warning, field situation and other monitoring information. If you think

the warning information is true and reliable, immediately start the prevention and control measures. If you think the warning information is not reliable

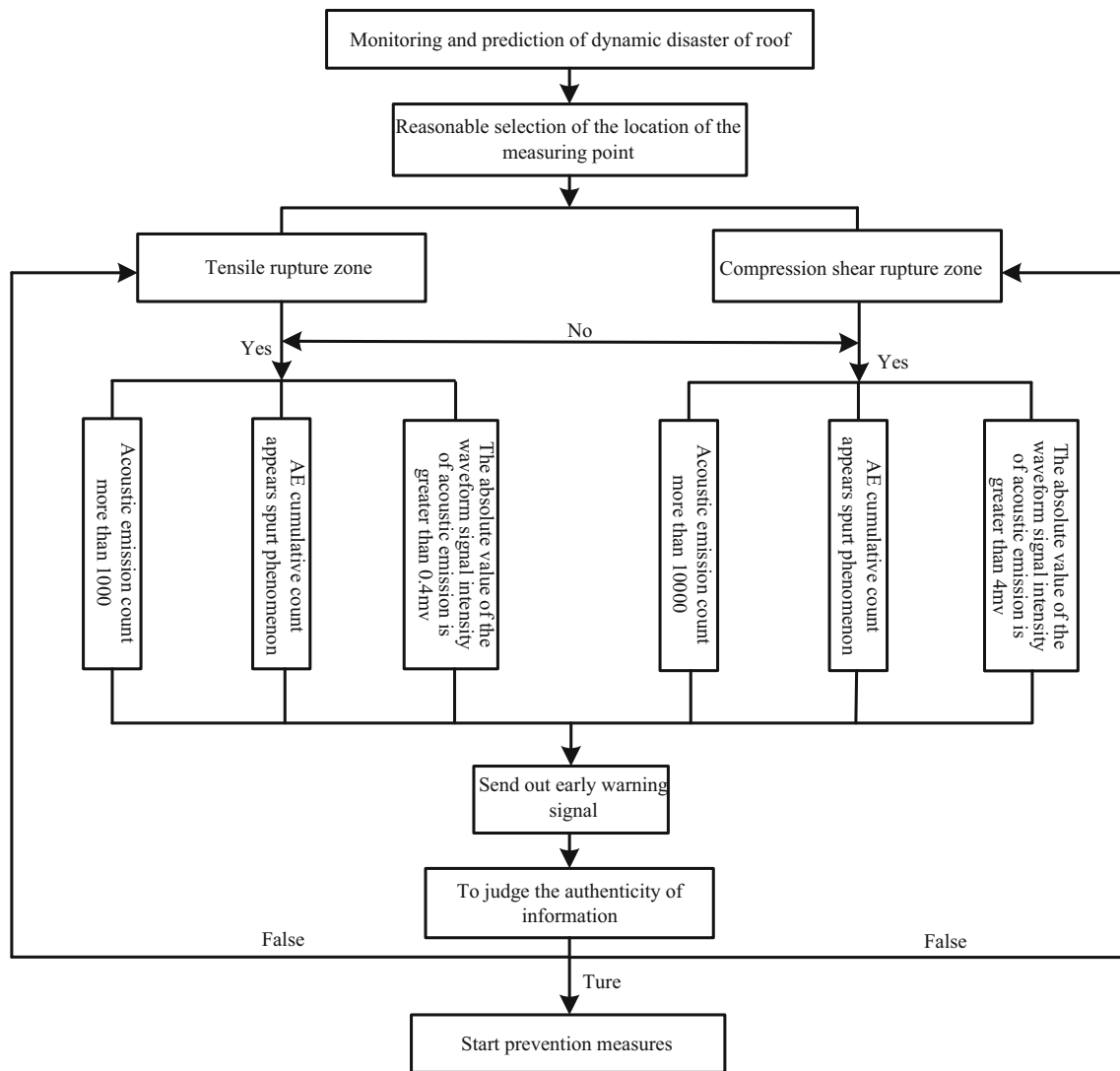


Fig. 13 Technical route of the predicting and forecasting on the thick hard roof dynamic disaster based on acoustic emission characteristics

after the judgment, release the pre-warning information and return to the monitor.

### 7 Conclusions

In order to explore the internal causes of dynamic disaster of thick hard roof sandstone and the prediction method of dynamic disaster, samples of thick hard roof sandstone were taken as the research object. The composition and microstructure of sandstone were investigated by using SEM and X-ray diffractometer. Finally, the mechanical and acoustic emission characteristics of sandstone were studied by using a RMT-150C mechanical testing machine and acoustic emission monitor. The result of analyses show that

- (1) The tensile strength, uniaxial compressive strength, elastic modulus and Poisson’s ratio of the roof sandstone are 4.825, 85.313 MPa, 13.814 GPa and 0.254, respectively. The cohesive strength and internal friction angle of the roof sandstone are 23.389 MPa and 32, respectively. The roof sandstone is a hard rock.
- (2) The cumulative counts of AE for the roof sandstone in the indirect tensile test, uniaxial compression test and triaxial compression test can be divided into three phases including the relatively flat growth period, the rapid growth period and the spurt period.
- (3) The intensities of AE signal in the tensile failure zone and in the compression shear failure zone have obvious difference. In the indirect tensile test, the signal intensity of acoustic emission waveform is

relatively low. However, the signal intensity of acoustic emission waveform is relatively large in the uniaxial compression test. Before the occurrence of fracture, the peak signal intensity of acoustic emission waveform is 0.8 and 10 mV, respectively.

- (4) In the tensile fracture zone, the precursor information of acoustic emission in the fracturing process of roof includes acoustic emission count more than 1000, AE cumulative counts appear to spurt and the absolute value of the waveform signal intensity of acoustic emission is greater than 0.4 mv. In the tensile fracture zone, the precursor information of acoustic emission in the fracturing process of roof includes acoustic emission count more than 10,000, AE cumulative counts appear to spurt and the absolute value of the waveform signal intensity of acoustic emission is greater than 4 mV.

**Acknowledgments** This research is funded by the Chinese Natural Science Committee under Grant No. U1261207.

**Open Access** This article is distributed under the terms of the Creative Commons Attribution 4.0 International License (<http://creativecommons.org/licenses/by/4.0/>), which permits unrestricted use, distribution, and reproduction in any medium, provided you give appropriate credit to the original author(s) and the source, provide a link to the Creative Commons license, and indicate if changes were made.

## References

- Chen TF, Xu JY, Liu S, Zhi LP (2013) Experimental study on ultrasonic and mechanical properties of sandstone influenced by water-saturation and high temperature. *Chin J Undergr Space Eng* 9(6):1236–1241
- Deng HF, Yuan XF, Li JL, Luo Q, He M (2014) Fracture mechanics characteristics and deterioration mechanism of sandstone under reservoir immersion interaction. *Earth Sci J China Univ Geosci* 39(1):108–114
- Deng HF, Zhou ML, Li JL, Hu YY, Xiao ZY, Wang Y (2016) Experimental research on unloading triaxial rheological mechanical properties of sandy mudstone. *Rock Soil Mech* 37(2):315–322
- Fang JY, Dang FN, Xiao YT, Ding WH, Fang JX (2015) Quantitative study on the CT test process of siltstone under triaxial compression. *Chin J Rock Mech Eng* 34(10):1976–1984
- Gao BB, Li HG, Li HM (2015a) Study on acoustic emission and fractal characteristics of different damage types of rock. *Chin J Undergr Space Eng* 11(2):358–363
- Gao BB, Li HG, Li HM, Li L, Su CD (2015b) Acoustic emission and fractal characteristics of saturated coal samples in the failure process. *J Min Saf Eng* 32(4):665–670
- Guo XF, Yin JM, Yan EC, Zhang LJ (2016) Mechanical property test at different unloading velocities of metamorphic quartz sandstone. *J Shanghai Jiao Tong Univ* 50(1):78–83
- Han TC, Zhang J (2014) Numerical simulation of acoustic emission for defective rock. *Chin J Rock Mech Eng* 33(supp1):3198–3204
- Li M (2014) Research on rupture mechanisms of coal measures sandstone under high temperature and impact load. China Univ Min Technol China, Xuzhou (Chinese)
- Li DY, Qiu JD, Li XB (2015a) Experimental study on dynamic tensile and compressive properties of bedding sandstone under impact loading. *Chin J Rock Mech Eng* 34(10):2091–2097
- Li HM, Li HG, Gao BB, Jiang DJ, Feng JF (2015b) Study of acoustic emission and mechanical characteristics of coal samples under different loading rates. *Shock Vib* 2015:1–11
- Liu JP, Xu SD, Li YH, Dong LB, Wei J (2012) Studies of AE time-space evolution characteristics during failure process of rock specimens with prefabricated holes. *Chin J Rock Mech Eng* 31(12):2538–2547
- Liu XL, Li XB, Hong L, Yin TB, Rao M (2015) Acoustic emission characteristics of rock under impact loading. *J Cent South Univ* 22:3571–3577
- Sachan A, Penumadu D (2007) Identification of microfabric of kaolinite clay mineral using X-ray diffraction technique. *Geotech Geol Eng* 25(6):603–616
- Su HJ, Jing HW, Zhao HH, Wang YC (2014) Experimental study on the influence of longitudinal fissure on mechanics characteristic of sandstone. *J Min Saf Eng* 31(4):644–649
- The Ministry of Water Resources of the People's Republic of China (2008) GB50487-2008 Code for Water Resources and Hydro-power Engineering Geological Investigation. China Planning Press, Beijing
- Wang SY, Sloan SW, Tang CA (2013) Three-dimensional numerical investigations of the failure mechanism of a rock disc with a central or eccentric hole. *Rock Mech Rock Eng* 47(6):1–21
- Wasantha PLP, Ranjith PG, Zhao J, Shao SS, Permata G (2015) Strain rate effect on the mechanical behavior of sandstones with different grain sizes. *Rock Mech Rock Eng* 48:1883–1895
- Yang SQ, Huang YH, Jing HW, Liu XL (2014) Discrete element modeling on fracture coalescence behavior of red sandstone containing two unparallel fissures under uniaxial compression. *Eng Geol* 178:28–48
- Yang SQ, Jing HW, Cheng L (2015) Influences of pore pressure on short-term and creep mechanical behavior of red sandstone. *Eng Geol* 179:10–23
- Yao QL, Li XH, Pan F, Weng T, Wang G (2016) Deformation and failure mechanism of roadway sensitive to stress disturbance and its zonal support technology. *Shock Vib* 2016:1–14
- Zhang YB, Mao XB, Tao J, Li M (2014) Impact of strain rate on mechanical property of sandstone under impact load. *Blasting* 31(3):42–46
- Zhang AB, Zhang YB, Liu XX, Zhang P (2015) Test study on water affected to physical mechanics performances of muddy siltstone. *Coal Sci Technol* 43(8):67–71
- Zhang C, Zhang AB, Zhang YB, Liu XX, Chen L (2016) Acoustic emission and damage evolution of dry and water-saturated. *J Liaoning Tech Univ (Nat Sci)* 35(7):705–711
- Zhou KP, Li B, Li JL, Deng HW, Bin F (2015) Microscopic damage and dynamic mechanical properties of rock under freeze-thaw environment. *Trans Nonferrous Metals Soc China* 25:1254–1261
- Zhu TT, Jing HW, Su HJ, Ying Q (2015) Experimental investigation on mechanical behavior of sandstone with coupling effects under uniaxial compression. *J China Coal Soc* 40(7):1518–1525